





Limitation of sucrose biosynthesis shapes carbon partitioning during plant cold acclimation

Anastasia Kitashova¹  | Stephan O. Adler² | Andreas S. Richter³  |
Svenja Eberlein¹ | Dejan Dziubek¹ | Edda Klipp²  | Thomas Nägele¹ 

¹Plant Evolutionary Cell Biology, Faculty of Biology, Ludwig-Maximilians-Universität München, Planegg-Martinsried, Germany

²Theoretical Biophysics, Institute of Biology, Humboldt-Universität zu Berlin, Berlin, Germany

³Institute for Biosciences, Physiology of Plant Metabolism, University of Rostock, Rostock, Germany

Correspondence

Thomas Nägele, Plant Evolutionary Cell Biology, Faculty of Biology, Ludwig-Maximilians-Universität München, Planegg-Martinsried, Germany.
Email: thomas.naegele@lmu.de

Funding information

Deutsche Forschungsgemeinschaft, Grant/Award Numbers: TR175/C06, TR175/D03

Abstract

Cold acclimation is a multigenic process by which many plant species increase their freezing tolerance. Stabilization of photosynthesis and carbohydrate metabolism plays a crucial role in cold acclimation. To study regulation of primary and secondary metabolism during cold acclimation of *Arabidopsis thaliana*, metabolic mutants with deficiencies in either starch or flavonoid metabolism were exposed to 4°C. Photosynthesis was determined together with amounts of carbohydrates, anthocyanins, organic acids and enzyme activities of the central carbohydrate metabolism. Starch deficiency was found to significantly delay soluble sugar accumulation during cold acclimation, while starch overaccumulation did not affect accumulation dynamics but resulted in lower total amounts of sucrose and glucose. Anthocyanin amounts were lowered in both starch deficient and overaccumulating mutants. Vice versa, flavonoid deficiency did not result in a changed starch amount, which suggested a unidirectional signalling link between starch and flavonoid metabolism. Mathematical modelling of carbon metabolism indicated kinetics of sucrose biosynthesis to be limiting for carbon partitioning in leaf tissue during cold exposure. Together with cold-induced dynamics of citrate, fumarate and malate amounts, this provided evidence for a central role of sucrose phosphate synthase activity in carbon partitioning between biosynthetic and dissimilatory pathways which stabilizes photosynthesis and metabolism at low temperature.

KEYWORDS

Arabidopsis thaliana, carbon metabolism, cold acclimation, kinetic modelling

1 | INTRODUCTION

Exposing plants to a changing temperature regime has an immediate effect on cellular metabolism. If temperature drops or increases severely within a short period, for example, within minutes, a stress response is induced to counteract and prevent irreversible cell and

tissue damage (Kosová et al., 2011). If significant acute damage and death can be prevented, metabolism is adjusted to a new homeostasis within a process termed acclimation. Temperature acclimation, and, more specifically, cold acclimation, is a multigenic process which comprises and affects the expression of thousands of genes (Fowler & Thomashow, 2002; Hannah et al., 2005) and abundance of

This is an open access article under the terms of the Creative Commons Attribution-NonCommercial License, which permits use, distribution and reproduction in any medium, provided the original work is properly cited and is not used for commercial purposes.

© 2022 The Authors. *Plant, Cell & Environment* published by John Wiley & Sons Ltd.

hundreds of metabolites (Cook et al., 2004; Kaplan et al., 2004). Many plant species from temperate regions are able to acclimate to low temperature which results in increased freezing tolerance (Xin & Browse, 2000). For *Arabidopsis thaliana*, it has been shown earlier that low temperature represents an important selective pressure, which indicates the significance of cold acclimation for plant evolution and ecology (Hannah et al., 2006).

Carbohydrates are direct products of photosynthetic CO₂ assimilation and their metabolism needs tight regulation to stabilize photosynthetic efficiency under changing environmental conditions. Primary reactions of photosynthesis are catalysed by photosystems II and I which trap and transform light energy into redox potential energy and a proton gradient. This enables biosynthesis of NADPH and ATP, respectively, being essential for carbon fixation within the Calvin–Benson–Bassham cycle (CBBC). Stabilizing the balance within this reaction network and energy flow is essential for plant cold acclimation (Leonardos et al., 2003). Chilling temperatures between 5°C and 10°C were found to inhibit photosynthetic carbon fixation, for example, due to inactivation of regulatory thioredoxin-activated enzymes of the CBBC (Holaday et al., 1992). Such a reduced CO₂ fixation rate may cause a significant imbalance between light absorption and energy consumption within the CBBC (Huner et al., 1998). To prevent limitations in carbohydrate metabolism, CBBC enzymes and enzymes of the sucrose biosynthesis pathway are tightly regulated on the transcriptional, translational and protein level during cold acclimation (Nägele et al., 2012; Stitt & Hurry, 2002; Strand et al., 2003). This enables plants to significantly accumulate soluble sugars during cold exposure which have been discussed to stabilize metabolism and to have a cryoprotective function (Klotke et al., 2004; Ristic & Ashworth, 1993; Seydel et al., 2022).

In chloroplasts, triose and hexose phosphates are direct CBBC products which serve as substrates for diverse biosynthetic pathways. Starting from fructose-6-phosphate, transient leaf starch is (diurnally) biosynthesised in a sequential reaction catalysed by phosphoglucosyltransferase (PGT), phosphoglucosyltransferase (PGT), ADP-glucose pyrophosphorylase and starch synthase enzymes (Stitt & Zeeman, 2012). During the night, starch is degraded by glucan/water dikinase and phosphoglucan/water dikinase enzymes to yield glucans (Kötting et al., 2005). Glucans are substrate for amylase enzymes yielding maltose moieties. Maltose is exported to the cytosol to supply carbon metabolism (Niittylä et al., 2004; Smith et al., 2005). Previously it was discussed that, during initial cold exposure, starch amount is transiently reduced to stabilize soluble sugar concentrations (Sicher, 2011). Evidence has also been provided for a role of starch degradation in the acquisition of freezing tolerance (Yano et al., 2005). Starch degradation in chloroplasts needs activity of β -amylases. In *Arabidopsis*, nine *BAM* genes have been described, and expression of *BAM3* (*ct-BMY*, *BMY8*, At4g17090) was found to be induced by cold stress (Kaplan & Guy, 2004; Monroe et al., 2014). In addition, relative protein levels of *BAM3* were found to be differentially regulated in freezing

sensitive and -tolerant accessions of *A. thaliana* suggesting a central role in regulation of starch degradation during cold acclimation (Nagler et al., 2015).

Besides biosynthesis and metabolism of carbohydrates, a significant portion of plants' carbon flow may be directed through the shikimate pathway, resulting in diverse metabolic products comprising aromatic amino acids, phytohormones and secondary metabolites. The entry reaction of the shikimate pathway has been shown to be tightly regulated (Yokoyama et al., 2021). Phosphoenolpyruvate and erythrose-4-phosphate from glycolysis and pentose phosphate pathways are interconverted into chorismate which represents the precursor of tryptophan, tyrosine and phenylalanine. Phenylalanine is precursor for flavonoid biosynthesis via the phenylpropanoid pathway which is located to the cytosol. Chalcone synthase (CHS) catalyses the first committed step in flavonoid biosynthesis forming chalcone by intramolecular cyclization and aromatization of a linear phenylpropanoid tetraketide (Austin & Noel, 2003). Plants were estimated to produce several thousands of structurally different flavonoids fulfilling a huge diversity of molecular and physiological functions (Falcone Ferreyra et al., 2012; Ferreyra et al., 2021; Winkel-Shirley, 2001, 2002). The reaction product of CHS, tetrahydroxychalcone, is the substrate for naringenin synthesis, catalysed by chalcone isomerase. Naringenin represents a central precursor for subgroups of flavonoids, which comprise flavones, flavonols, flavandiols, anthocyanins and proanthocyanidins (Winkel-Shirley, 2002). Early steps of anthocyanin biosynthesis comprise the interconversion of naringenin into dihydroflavanol, catalysed by flavanone 3-hydroxylase (F3H) together with flavonoid 3'-hydroxylase (Owens et al., 2008; Shi & Xie, 2014). Enhanced dynamics of flavonoid metabolism have previously been associated with cold and freezing tolerance (Hannah et al., 2006; Korn et al., 2008; Schulz et al., 2015, 2016). Anthocyanins were suggested to have a photoprotective role at chilling temperature (Havaux & Klopstsch, 2001), and by accumulation in the vacuole they were discussed to affect osmotic potential and prevent tissue damage due to freezing (Chalker-Scott, 1999).

While a tightly regulated allocation of photosynthetically fixed carbon between pathways of primary and secondary metabolism seems essential for plant growth, development and stress response (Caretto et al., 2015), underlying metabolic regulation remains elusive. Particularly, under a changing temperature regime, thermodynamic constraints of enzyme activity and metabolic regulation result in a non-linear output of metabolic systems, that is, metabolic regulation, which prevents intuitive interpretation and hypothesis generation of experimental observations. In the present study, kinetics of carbohydrate and anthocyanin accumulation were quantitatively monitored during cold acclimation to reveal regulatory interactions between starch, sucrose and anthocyanin metabolism. Enzyme kinetic modelling was applied to study the effect of low temperature on kinetics of carbon allocation. Finally, analysis of metabolic mutants provided evidence for dynamic carbon partitioning between primary and secondary metabolism during cold acclimation.

2 | MATERIALS AND METHODS

2.1 | Plant material and growth conditions

Plants of *A. thaliana* accession Col-0 and homozygous T-DNA insertion lines *bam3* (beta-amylase 3, line SALK_041214, locus AT4G17090), *chs* (line SALK_020583C, locus AT5G13930), *f3h* (flavanone 3-hydroxylase, line SALK_113904C, locus AT3G51240), as well as SNP mutant *pgm1* (plastidial PGM, TAIR stock CS3092, locus AT5G51820) were grown on a 1:1 mixture of GS90 soil and vermiculite in a climate chamber under controlled short-day conditions (8 h/16 h light/dark; 90–100 $\mu\text{mol m}^{-2} \text{s}^{-1}$; 22°C/16°C; 60% relative humidity). All seeds were harvested from plants grown in one batch, that is, at the same time and under same conditions. After 4 weeks, plants were shifted to a growth cabinet and grown further under long day conditions (16 h/8 h light/dark; 90–100 $\mu\text{mol m}^{-2} \text{s}^{-1}$; 22°C/16°C; 60% relative humidity). After 2 weeks, plants were either (i) harvested at midday, that is, 8 h of light (0 days of cold acclimation) or (ii) transferred to a cold room for cold acclimation (16 h/8 h light/dark; 90–100 $\mu\text{mol m}^{-2} \text{s}^{-1}$; 4°C/4°C). Cold exposed plants were harvested after 1, 3, 7 or 14 days of acclimation at midday, that is, after 8 h of light. Each sample consisted of nine leaf rosettes which were immediately frozen in liquid nitrogen, ground to a fine powder and lyophilised. The rather low to moderate photosynthetic active radiation (PAR) intensity of 90–100 $\mu\text{mol m}^{-2} \text{s}^{-1}$ was applied to minimize photoinhibition and to prevent mixed effects of cold and light acclimation. Relative proportion of UV radiation in growth chambers was 0.3 – 0.5% of total photon flux density (LICOR LI-180 Spectrometer; www.licor.com).

2.2 | RNA extraction and qPCR analysis

Whole leaf RNA was extracted as described earlier (Oñate-Sánchez & Vicente-Carbajosa, 2008). Frozen and ground leaf material was resuspended in 300 μl cell lysis buffer (2% [wt/vol] sodium dodecyl sulphate, 68 mM sodium citrate, 132 mM citric acid, 1 mM EDTA), 100 μl DNA/protein precipitation solution were added (4 M NaCl, 16 mM sodium citrate, 32 mM citric acid), and samples were vortexed and incubated on ice for 10 min. Samples were centrifuged at 13 000 rpm (4°C) for 10 min, and 300 μl of the supernatant were used to precipitate the RNA with 300 μl isopropanol. Pellets were washed with 800 μl 75% ethanol, centrifuged and dried. The RNA was resuspended in 20–25 μl of H₂O (RNase free) and stored at –80°C until further use.

For qPCR analysis, 1–2 μg of DNaseI (Thermo Fisher Scientific) treated RNA was transcribed into cDNA using RevertAid reverse transcriptase (Thermo Fisher Scientific) according to the manufacturer protocol. The qPCR analysis was performed in a CFX96-C1000 96-well plate thermocycler (Bio-Rad) and ChamQ Universal SYBR qPCR Master Mix (Absource) in 6 μl reactions containing 1 μl of diluted (1:5) cDNA. Relative gene expression was calculated using the $2^{-\Delta\Delta\text{Ct}}$ method and SAND (AT2G28390) as the reference gene.

2.3 | Net photosynthesis and chlorophyll fluorescence measurements

Rates of net CO₂ assimilation, that is, net photosynthesis (NPS), were recorded for 1 h at midday in 15 min intervals using a WALZ GFS-3000FL system (Heinz Walz GmbH; www.walz.com). Maximum quantum yield of PSII (F_v/F_m) was determined after 10 min of dark adaptation by supplying a saturating light pulse, which was tested to be suitable for the following experimental setup. Dynamics of quantum efficiency of PSII ($\Phi(\text{II})$), electron transport rate (ETR), photochemical (qP, qL), non-photochemical quenching (qN, NPQ), quantum yield of regulated energy dissipation (Y(NPQ)) and quantum yield of nonregulated energy dissipation (Y(NO)) were determined either (i) within rapid stepwise increase of PAR from 0 to 2400 $\mu\text{mol m}^{-2} \text{s}^{-1}$; or (ii) after 10 min of acclimation to ambient light, that is, 100 $\mu\text{mol m}^{-2} \text{s}^{-1}$, or saturating light, that is, 1200 $\mu\text{mol m}^{-2} \text{s}^{-1}$, using WALZ JUNIOR-PAM system (Heinz Walz GmbH; www.walz.com; Figure S1). NPS and chlorophyll fluorescence parameters were recorded at ambient temperature (22°C) for non-acclimated plants (0 days of acclimation) and at 4°C for cold acclimated plant (1, 3, 7 and 14 days of acclimation).

2.4 | Quantification of starch, soluble carbohydrates, hexose phosphates and anthocyanins

Transitory starch and soluble carbohydrates amounts were determined as described previously with slight modifications (Atanasov et al., 2020; Nägele et al., 2012). In brief, following extraction with 80% ethanol at 80°C for 30 min and short centrifugation, the supernatant was transferred to a new tube and extraction was repeated. Starch-containing pellets were incubated with 750 μl 0.5 N NaOH at 95°C for 60 min before slight acidification with 750 μl 1 M CH₃COOH. Glucose units resulting from digestions with amyloglucosidase were quantified photometrically applying a coupled glucose oxidase/peroxidase/dianisidine reaction which yielded a reaction product with a specific absorbance maximum at 540 nm.

Dried ethanol extracts were used for quantification of soluble carbohydrates, that is, glucose, fructose and sucrose. Glucose was quantified using a coupled hexokinase/glucose-6-phosphate dehydrogenase (G6PDH) assay, which yielded NADPH + H⁺ detectable at 340 nm. For fructose quantification, PGI was added to the reaction mix after glucose amount had been detected. Sucrose concentration was determined using an anthrone reagent composed of 14.6 M H₂SO₄ and 0.14% (wt/vol) anthrone. Samples were incubated with 30% KOH at 95°C before adding the anthrone reagent, incubating for 30 min at 40°C and detecting absorbance at 620 nm.

Glucose 6-phosphate (G6P) and fructose 6-phosphate (F6P) were quantified as described before (Gibon et al., 2002). G6P and F6P were extracted using trichloroacetic acid (TCA) in diethyl ether (16% wt/vol), washed with 16% (wt/vol) TCA in 5 mM EGTA and neutralised with 5 M KOH/1 M triethanolamine. G6P and F6P

concentration was determined using an enzymatic cycling assay, catalysing interconversion of hexose-phosphates into NADPH + H⁺, which was photometrically determined in a reaction with formazan dye at 570 nm.

Anthocyanins were quantified as described before (Atanasov et al., 2020). In brief, ground plant material was suspended in 1 N HCl and incubated at 25°C for 30 min while shaking. Following short centrifugation, supernatant was transferred to a new tube, and extraction was repeated at 80°C for 30 min. After a second centrifugation, supernatants were pooled and the amount of anthocyanins was quantified photometrically at 540 nm. Total anthocyanin concentration was normalised to pelargonidin standards (C₁₅).

2.5 | Quantification of enzyme activities

Activities of sucrose phosphate synthase (SPS), glucokinase, fructokinase, invertase and PGI were determined under substrate saturation (v_{\max}) at 4°C and 22°C.

Maximal activity of SPS was determined as described earlier (Nägele et al., 2012). Ground plant material was suspended in extraction buffer containing 50 mM HEPES-KOH (pH 7.5), 10 mM MgCl₂, 1 mM EDTA, 2.5 mM DTT, 10% (vol/vol) glycerine and 0.1% (vol/vol) Triton X-100. After incubation on ice and centrifugation, the supernatant was incubated for 30 min at 22°C or 50 min at 4°C with reaction mixture consisting of 50 mM HEPES-KOH (pH 7.5), 15 mM MgCl₂, 2.5 mM DTT, 35 mM UDP-glucose, 35 mM F6P and 140 mM G6P. The reaction was stopped by adding 30% KOH and heating samples to 95°C. Sucrose concentration was detected in the anthrone assay as described above.

Neutral (nINV) and acidic (aINV) invertase activities were quantified as described previously with slight modification (Nägele et al., 2012). Ground plant material was suspended in 50 mM HEPES-KOH (pH 7.5), 5 mM MgCl₂, 2 mM EDTA, 1 mM phenylmethylsulfonylfluoride, 1 mM DTT, 10% (vol/vol) glycerine and 0.1% (vol/vol) Triton X-100 buffer. After incubation on ice and centrifugation, supernatants were desalted using Sephadex G-25 Medium. Activity of nINV was determined using a reaction buffer with pH 7.5 (20 mM HEPES-KOH, 100 mM sucrose), aINV activity was determined at pH 4.7 (20 mM sodium acetate, 100 mM sucrose). After incubation of the reaction mixture at 22°C or 4°C, reaction was stopped by heating to 95°C, and glucose moieties were photometrically determined with a coupled glucoseoxidase/peroxidase/dianisidine reaction to yield a reaction product with specific absorbance maximum at 540 nm.

Activities of gluco- and fructokinase (GLCK, FRCK) were determined as described before with slight modification (Wiese et al., 1999). Following suspension of ground plant material in extraction buffer containing 50 mM Tris-HCl (pH 8.0), 0.5 mM MgCl₂, 1 mM EDTA, 1 mM DTT and 1% (vol/vol) Triton X-100, samples were incubated on ice and then centrifuged. The supernatant was mixed with reaction mix containing 100 mM HEPES-KOH

(pH 7.5), 10 mM MgCl₂, 2 mM ATP, 1 mM NADP⁺, 0.5 U G6PDH and either 5 mM glucose for glucokinase measurement or 5 mM fructose for fructokinase measurement. Produced NADPH was recorded photometrically at 340 nm for 20 min for measurements at 22°C, and for 60 min for measurements at 4°C. Activities were derived from slopes of absorbances.

PGI maximal activity was determined as described before (Kitashova et al., 2021). Ground plant material was suspended in extraction buffer containing 50 mM Tris-HCl (pH 8.0), 0.5 mM MgCl₂, 1 mM EDTA, 1 mM DTT and 1% (vol/vol) Triton X-100. Following incubation on ice and centrifugation, supernatants were mixed with 100 mM HEPES-KOH (pH 7.5), 10 mM MgCl₂, 1 mM NADP⁺ and 0.5 U G6PDH. After addition of 50 mM F6P slopes of NADPH + H⁺ were recorded photometrically at 340 nm for 10 min for quantifying v_{\max} 22°C, and for 45 min for quantification at 4°C.

Total amylase (AMY) activity was measured at 22°C following the SIGMA-ALDRICH Amylase Activity Assay Kit protocol, catalogue number MAK009 (www.sigmaaldrich.com). Amylase was extracted with Amylase Assay Buffer on ice and after short centrifugation it was mixed with the Master Reaction Mix. Absorbance at 405 nm was recorded every minute for 15 min.

Activation energy (E_a) was determined from the slope ($-E_a/R$; R is the gas constant) of a linear graph describing natural logarithm of v_{\max} ($\ln v_{\max}$) as a function of inverse temperature ($1/T$). This was based on a logarithmic conversion of the Arrhenius equation (Arrhenius, 1889), that is, $\ln v_{\max} = (-E_a/R) \times (1/T) + \ln A$ where the constant A represents the probability of reaction (Bisswanger, 2008).

2.6 | Quantification of organic acids

Organic acids citrate, fumarate and malate were extracted from freeze-dried plant material using hot water and incubating samples at 95°C for 15 min. After short centrifugation, supernatants were used for organic acid amount quantification with SIGMA-ALDRICH Assay Kits (catalogue numbers MAK057, MAK060 and MAK067). Citrate was quantified by incubating the supernatant with Citrate Enzyme Mix, Citrate Developer and Probe Solution in Citrate Assay Buffer in darkness at 22°C for 30 min and recording absorbance at 570 nm. Fumarate concentration was estimated after incubating the supernatant with the Fumarate Enzyme Mix and Fumarate Enzyme Mix in Fumarate Assay Buffer in darkness at 22°C for 30 min and measuring absorbance at 450 nm. Malate amount was detected after incubating the supernatant with the Malate Enzyme Mix and WST Substrate Mix in Malate Assay Buffer in darkness at 37°C for 30 min and measuring absorbance at 450 nm.

2.7 | Statistics and mathematical modelling

Statistical data evaluation was done using the free software environment R Version 3.6.2 (www.r-project.org) (R Core Team 2019) and RStudio Version 1.2.5033 (www.rstudio.com) (RStudio

Team 2019). Mathematical modelling was performed in MATLAB Version 9.10.0.1739362 (R2021a) (www.mathworks.com) with the toolbox IQM Tools developed by IntiQuan (www.intiquan.com). Parameter estimation was performed applying a particle swarm pattern search method for bound constrained global optimization (Vaz & Vicente, 2007). The cost function (also: objective function) $f(z)$ quantified the discrepancy between simulated and experimental metabolite amounts and was minimized within the optimization problem $\min_{z \in \mathbb{R}^n} f(z)$, $z \in \Omega$, with $\Omega = \{z \in \mathbb{R}^n : l \leq z \leq u\}$.

For model simulations of cold exposed plants, v_{\max} quantified at 4°C was used. Kinetic parameters not experimentally quantified in the present study, that is, K_M and K_i values, were derived from literature, for example, Kitashova et al. (2021), Nägele et al. (2012), Weiszmann et al. (2018).

A graphical illustration of the mathematical model describing the central carbohydrate metabolism is provided (Figure 1), and Figure SII extended this model by an additional F6P consumption pathway, termed r_2 . The model was based on a system of ordinary differential equations which is described in detail in the supplements (Tables SI and SII). Rates of net photosynthesis ($rNPS$) were calculated as the average rate of carbon uptake at midday, that is, after 8 h of light.

Starch was assumed to be synthesised with a constant average rate ($rSTAsyn$) during the first 8 h of light which finally resulted in the quantified amount of non-acclimated plants (0 day). For cold-exposed plants, the net rate of starch biosynthesis was calculated as the difference of starch amount between the day considered and the preceding sampling time point. This revealed the net flux of starch within the system between two sampling time points, that is, for Day 1 at 4°C: $([starch_{\text{amount},1d} - starch_{\text{amount},0d}]/24 \text{ h})$, for Day 3 at 4°C:

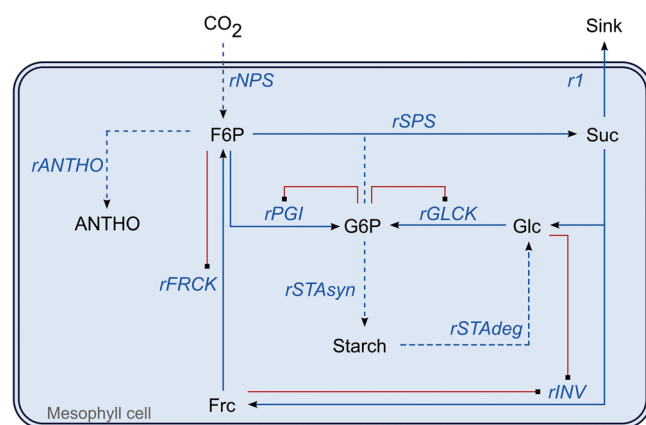


FIGURE 1 Graphical representation of the central carbohydrate metabolism. Blue arrows represent enzyme reactions, red lines represent inhibition. F6P, fructose-6-phosphate; G6P, glucose-6-phosphate; ANThO, anthocyanins; Glc, glucose; Frc, fructose; Suc, sucrose; $rNPS$, rate of net photosynthesis; $rANThO$, rate of anthocyanin biosynthesis; $rSTAsyn$, rate of starch biosynthesis; $rSTAdeg$, rate of starch degradation; $rSPS$, rate of sucrose phosphate synthase; $rPGL$, rate of phosphoglucosomerase; $rINV$, rate of invertase; $rGLCK$, rate of glucokinase; $rFRCK$, rate of fructokinase; r_1 , rate of sucrose export to sinks.

$([starch_{\text{amount},3d} - starch_{\text{amount},1d}]/48 \text{ h})$, and so on. Also, rates of anthocyanin accumulation ($rANThO$) were calculated as change in net concentration per day.

Models of all genotypes and acclimation time points are provided in SBML format in the supplements (File SBML models). Models with a suffix "exp2" indicate extended model structures comprising a second export rate r_2 (see explanation above).

3 | RESULTS

3.1 | Photosynthetic activity during cold acclimation

Chlorophyll fluorescent parameters and $rNPS$ were quantified to reveal effects of mutation in starch or flavonoid metabolism during cold acclimation (Figures 2 and 3). Generally, cold exposure resulted in a significant reduction of maximum quantum yield of PSII (F_v/F_m), ETR, effective PSII yield ($\Phi(II)$) and photochemical quenching (qP , qL ; Figures 2 and SIII; Table SIIIA). Only in the $f3h$ mutant, a slight decrease of F_v/F_m was observed from 1 to 3 days of cold acclimation, which recovered again to values higher at 14 days than after 7 days of acclimation (Figure 2). In $bam3$, F_v/F_m tended to increase during 14 days at 4°C after a significant drop at Day 1, while $pgm1$ had slightly lower F_v/F_m during the full acclimation periods compared to all other genotypes.

Rapid light curves were recorded to quantify the effect of rapidly increasing light intensities under low temperature on photosynthetic efficiencies (Figures SIII and SIV). Here, quantum yield of nonregulated energy dissipation ($Y(NO)$), a measure for negative effects of cold on photochemical energy conversion, was significantly increased in all cold-acclimated plants (Figure SIV; Table SIIIA). In addition to rapid light curve measurements, chlorophyll fluorescence was also monitored in steady state conditions after acclimation to ambient and high/saturating light, that is, 100 and 1200 μE , respectively (Figure SV; Table SIIIB). Under saturating light, fluctuation of qN , NPQ and $Y(NPQ)$ was more pronounced in mutants than in Col-0 between 1 and 7 days of cold acclimation (Figure SV). Finally, after

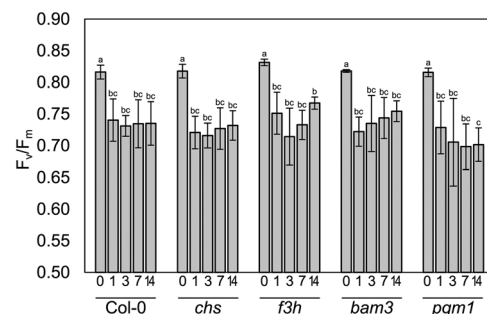


FIGURE 2 Maximum quantum yield of PSII in Col-0, chs , $f3h$, $bam3$ and $pgm1$ after 0, 1, 3, 7 and 14 days at 4°C. Bars represent means \pm standard deviation, letters indicate significantly different groups (ANOVA with Tukey HSD, $p < 0.05$; $n \geq 5$).

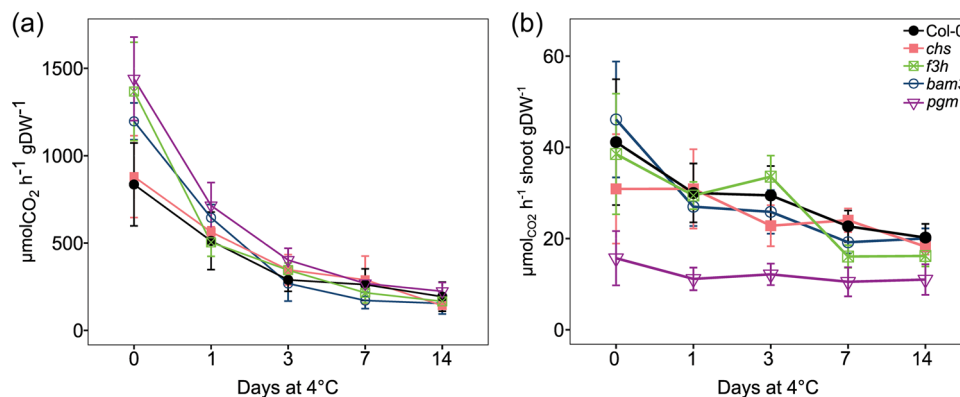


FIGURE 3 (a) Net CO₂ assimilation rates normalised to 1 g dry weight, and (b) net CO₂ assimilation rates of whole plant shoots in Col-0, *chs*, *f3h*, *bam3* and *pgm1* at 0, 1, 3, 7 and 14 day of cold acclimation. ● (black) represents Col-0; □ (pink): *chs*; ⋈ (green): *f3h*; ◊ (blue): *bam3*; ▽ (purple): *pgm1*. Vertical bars represent standard deviation, $n > 3$. [Color figure can be viewed at wileyonlinelibrary.com]

14 days, qN, NPQ and Y(NPQ) reached higher values in Col-0 than in *chs*, *f3h*, *bam3* and *pgm1*.

Rates of net CO₂ fixation normalised to (1 g) dry weight were significantly and immediately decreasing during cold exposure (Figure 3a). Despite differences in non-acclimated plants (Table SIIIA), all mutants had wild-type-like assimilation rates during cold acclimation. Interestingly, when normalised to the dry weight of the whole plant shoot, the cold-induced drop of net CO₂ assimilation rates was less pronounced, or even absent in *chs* (Figure 3b). In *pgm1*, shoot-normalised CO₂ assimilation rates were significantly lower than in Col-0 before and during cold exposure.

Quantifying fresh weight and dry weight of whole plant shoots during the cold acclimation period revealed different growth dynamics of genotypes (Figures SVI and SVII). As expected, dwarf *pgm1* plants had significantly lower shoot fresh and dry weight than all other genotypes but increased its shoot dry weight four- to fivefold within 14 days at 4°C. While fresh and dry weight were significantly positively correlated in Col-0 ($R = 0.76$, $p = 1.5e-07$), flavonoid-deficient mutants *f3h* and *chs* showed even more significant and stronger correlation of fresh and dry weight during cold acclimation (*f3h*: $R = 0.86$, $p = 1.1e-09$; *chs*: $R = 0.91$, $p = 1.8e-13$; Figure SVII).

3.2 | Dynamics of central carbohydrates and anthocyanins during cold acclimation

In plants of *f3h* and *chs* mutants, neither anthocyanins nor transcripts of the respective gene were accumulating during cold exposure (Figures 4A and SVIII; Table SIV). In plants of *bam3* and *pgm1*, anthocyanin dynamics were lowered at Days 7 and 14 at 4°C when compared to Col-0 (Figure 4A). Anthocyanin amount in Col-0 increased significantly by almost sixfold between 3 and 7 days at 4°C and dropped again significantly until 14 days of cold exposure. In plants of *bam3*, anthocyanins also increased strongest between 3 and 7 days in the cold but continued accumulating until 14 days at 4°C

reaching a final amount of ~15 μmol pelargonidin g DW⁻¹, which was ~75% of the wild-type amount (~20 μmol pelargonidin g DW⁻¹). In *pgm1*, anthocyanin amount peaked at Day 7 in the cold to an amount of ~15 μmol pelargonidin g DW⁻¹, which was approximately 50% of wild-type amount before it dropped again slightly until 14 days at 4°C.

Starch dynamics during cold exposure were similar across all tested genotypes except for *pgm1*, which was starch deficient (Figure 4b). Following a slight drop during the first day at 4°C, starch of Col-0, *f3h* and *chs* accumulated to three- to fourfold higher amounts until Day 7 in the cold compared to t(0), before slightly dropping at Day 14. Plants of *bam3* were observed to continuously accumulate starch during cold exposure and the final amount was about 1.5× higher than in Col-0 (Figure 4b). Sucrose amount significantly increased in all genotypes during the first 3 days at 4°C before it dropped significantly until Day 14 (Figure 4c). In *f3h* and *bam3*, sucrose amount increased slightly between 7 and 14 days in the cold, while it constantly decreased in *pgm1* after peaking at Day 3. While at 22°C (0 day) *pgm1* had almost double amount of sucrose, its cold-induced accumulation was delayed and resulted in a similar amount like in Col-0 after 14 days at 4°C (Figure 4c).

Similar to sucrose, also glucose and fructose amounts strongly increased during the first 3 days of cold exposure before it dropped again significantly until 14 days at 4°C (Figure 5a,b). In *chs* and *pgm1*, accumulation of glucose was delayed and reached its peak amount on day 7 at 4°C, which was, however, significantly lower than in Col-0 (Figure 5a). In *pgm1*, also fructose accumulation was delayed compared to Col-0, reaching a maximum after 7 days in the cold (Figure 5b).

Phosphorylation products of free hexoses, that is, glucose-6-phosphate (G6P) and fructose-6-phosphate (F6P), accumulated during the early phase of cold exposure (1–3 days) and particularly G6P stabilized quickly to a new homeostatic amount (Figure 5c,d). Flavonoid biosynthesis mutants *chs* and *f3h* accumulated slightly higher amounts of G6P at Day 1 in the cold, while *bam3* did not differ significantly from Col-0 (Figure 5c). Starch deficient *pgm1*, however,

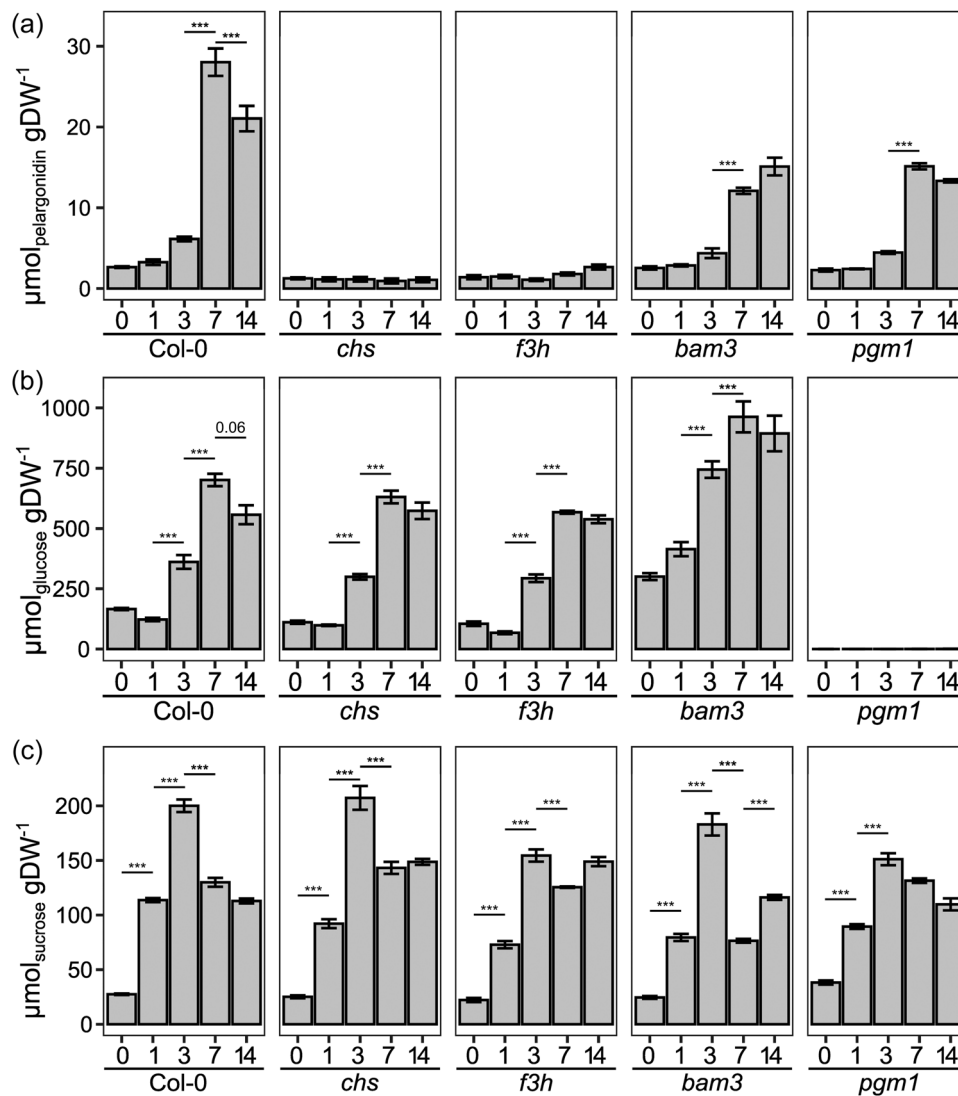


FIGURE 4 (a) Anthocyanin, (b) starch, and (c) sucrose dynamics in Col-0, *chs*, *f3h*, *bam3* and *pgm1* at 0, 1, 3, 7 and 14 days of cold acclimation. Bars represent means \pm SD. Asterisks indicate significant difference between consecutive days within one genotype: *** $p < 0.001$; ** $p < 0.01$; * $p < 0.05$ (ANOVA with Tukey HSD, $n \geq 5$).

showed the strongest accumulation of both G6P and F6P resulting in a ~ 3.5 -fold increase of G6P and approximately sevenfold increase in F6P after the first day of cold exposure (Figure 5c,d).

3.3 | Starch deficiency increases enzyme activities in central carbohydrate metabolism during cold acclimation

Maximum enzyme activity under substrate saturation (v_{\max}) was quantified at both 22°C and 4°C to compare (i) regulatory dynamics referencing to ambient temperature (22°C; Figure 6), and (ii) to estimate maximum in vivo flux capacities during cold exposure (4°C; Figure SIX). Both v_{\max} of glucokinase (GLCK) and fructokinase (FRCK) were found to be increased during cold exposure in Col-0 and *bam3* while remaining constant or even decreasing in *f3h* and *chs*,

respectively (Figure 6a,b). In *pgm1*, GLCK activity remained constant and FRCK activity significantly increased almost twofold after 14 days at 4°C (Figure 6b).

In Col-0 and *pgm1*, v_{\max} of PGI increased during the first day of cold exposure while it remained constant in all other genotypes (Figure 6c). After 3–7 days at 4°C, v_{\max} stabilized to a similar value as before cold exposure in all genotypes except for *pgm1* which showed a significant ~ 1.6 -fold increase until 14 days of cold exposure.

Compared to Col-0, all analysed mutants showed a significantly higher v_{\max} of SPS at ambient growth conditions (0 day 4°C; Figure 6d). Low temperature induced an increase of v_{\max} in Col-0 and *pgm1*, which resulted in a ~ 1.5 -fold increased SPS capacity after 14 days at 4°C in both genotypes. However, absolute activity in *pgm1* was constantly higher (approximately twofold) than in Col-0. In *bam3*, *chs* and *f3h*, cold induced a decrease in v_{\max} of SPS, resulting in wild-type-like activity after 7–14 days of cold exposure (Figure 6d).

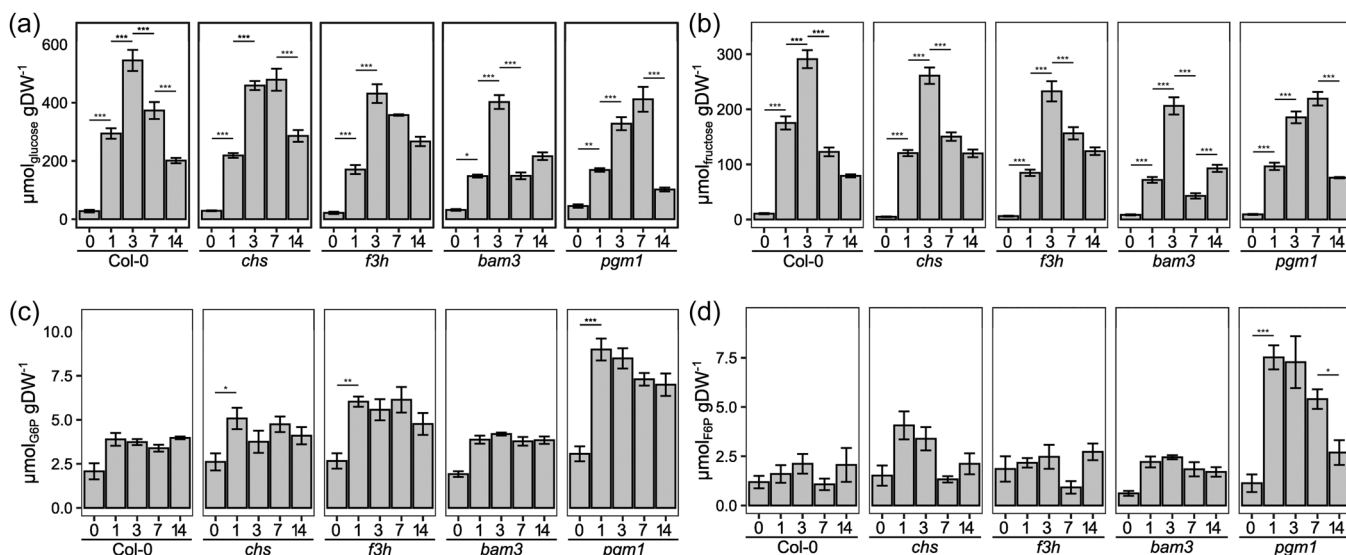


FIGURE 5 (a) Glucose, (b) fructose, (c) glucose-6-phosphate (G6P) and (d) fructose-6-phosphate (F6P) dynamics in Col-0, *chs*, *f3h*, *bam3* and *pgm1* at 0, 1, 3, 7 and 14 days of cold acclimation. Bars represent means \pm SD. Asterisks indicate significant difference between consecutive days within one genotype: *** $p < 0.001$; ** $p < 0.01$; * $p < 0.05$ (ANOVA with Tukey HSD, $n \geq 5$).

As observed for SPS, also v_{\max} of acidic (aINV) and neutral (nINV) invertase was found to be higher in metabolic mutants than in Col-0 before and, partially, also during cold exposure (Figure 6e,f). After 14 days at 4°C, v_{\max} of aINV was similar to Col-0 in all mutants (Figure 6e). For nINV, a similar trend was observed but *pgm1* and *f3h* had higher activities than the other mutants while no strong dynamics was found in Col-0, *chs* and *bam3* (Figure 6f).

Total amylase (AMY) activity quantification showed a fast cold-induced increase in all genotypes except for *bam3*, and the strongest dynamics was observed in Col-0 which reached a peak value already after 1 day at 4°C (Figure 6g). Prolonged cold exposure for 7 days resulted in decreased AMY activity in Col-0, *chs* and *f3h*. Starch deficient *pgm1* displayed a delayed increase of AMY v_{\max} reaching wild-type-like levels after 7 days. In plants of *bam3*, total AMY activity was found to be significantly lower than in Col-0 before cold acclimation (Table SV) and displayed reduced dynamics in total AMY activity during cold exposure.

Across all genotypes, maximum enzyme activities of PGI, SPS and aINV, quantified at 22°C, positively correlated with activities quantified at 4°C ($p < 0.05$, Pearson correlation with Benjamini–Hochberg p value adjustment; Figure SIX). In contrast, for GLCK, FRCK and nINV measurements at 22°C and 4°C were not observed to correlate, which suggested differential, and enzyme-specific, thermodynamic constraints. To systematically study temperature dependencies of (maximal) reaction rates, v_{\max} of GLCK, FRCK, PGI, SPS, aINV and nINV were quantified at 4°C, 8°C, 16°C and 22°C (i.e., 277.15, 281.15, 289.15 and 295.15 K) for non-acclimated Col-0 (Figure 7). Applying logarithmic conversion of the Arrhenius equation (see Section 2 for details) revealed activation energies, E_a , within an overall physiologically feasible range (e.g., for comparison: literature value of E_a for invertase [unspecific], 40–50 kJ mol⁻¹; Bisswanger, 2008). Notably, PGI and aINV regression could not

successfully reproduce all experimental observations both over-estimating v_{\max} at 16°C, that is, 289.15 K (Figure 7c,e).

3.4 | Parameter optimization of a kinetic model reveals differential cold-induced metabolic reprogramming

To quantitatively integrate net CO₂ assimilation rates, metabolite concentrations and enzyme activities, a kinetic model was developed comprising carbon input and output functions, starch and sugar metabolism as well as carbon export for secondary metabolism, that is, biosynthesis of anthocyanins (see Figure 1; Table SI; Supporting Information SBML model files). For each sampling time point of the experimental setup, models were optimized to simulate steady state metabolite concentrations being constrained by the input function ($rNPS$), enzyme parameters (v_{\max} , K_m , K_i), rates of starch biosynthesis and degradation ($rSTAsyn$, $rSTAdeg$) as well as net anthocyanin biosynthesis ($rANTHO$). Parameter optimization was evaluated by a cost function quantifying the (squared) error between simulated and experimentally quantified metabolite concentrations.

While the model structure could explain steady states in all genotypes before cold exposure (Day 0) with a low-valued cost function ($< 1 \times 10^{-9}$), the first day at 4°C could not be simulated within the experimentally observed standard deviations of both metabolite concentrations and enzyme parameters in neither genotype (cost function value $> 1 \times 10^5$; Figures 8a,b and SX). After 3 days at 4°C, parameter optimization for the *pgm1* model was successful again yielding simulations which reflected metabolite concentrations with a low cost function value (Figure 8b). For all other genotypes, parameter optimization was less successful until 7d (*bam3*) and 14 d (Col-0, *chs*, *f3h*), respectively.

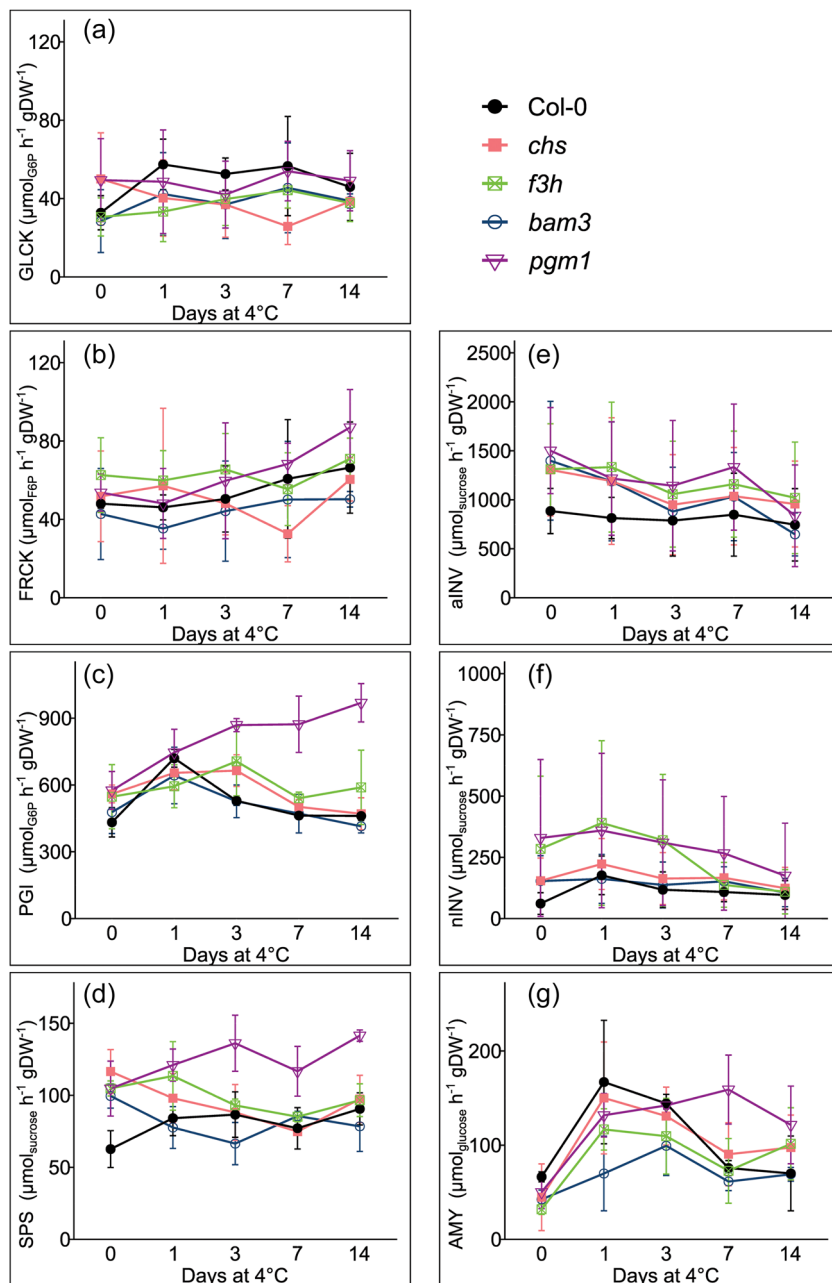


FIGURE 6 Maximum enzyme activities (v_{max}) at ambient temperature (22°C). (a) Glucokinase, GLCK; (b) fructokinase, FRCK; (c) phosphoglucosomerase, PGI; (d) sucrose-phosphate synthase, SPS; (e) acidic invertase, aINV; (f) neutral invertase, nINV; (g) amylase, AMY. ● (black) represents Col-0; ■ (pink): *chs*; ☒ (green): *f3h*; ○ (blue): *bam3*; ▽ (purple): *pgm1*. Vertical bars represent standard deviation, $n \geq 5$. [Color figure can be viewed at wileyonlinelibrary.com]

Comparison of parameter sets and optimization boundaries indicated a significant limitation of model solutions during cold acclimation by SPS-catalysed sucrose biosynthesis (Table SIV). In model simulations, sucrose amount was significantly lower than levels observed in experiments which suggested an unbalanced sucrose biosynthesis and sucrose cleavage or export to other pathways and/or organs (Figure SX: Days 1, 3 and 7). To overcome this limitation of parameter optimization, an additional (metabolic) sink was introduced representing any flux of F6P consumption which might result in other products than sucrose or starch, for example, organic and amino acids, or might supply respiration (Figure SII; Table SII; Supporting Information SBML model files). This structural change of the model improved model simulations and could successfully recover the simulation quality of experimental data, that is, lower the cost function values (Figure SXI; Table SVII). Based on previous

reports which showed that, under 4°C, organic acids like malate or fumarate significantly accumulate, also during initial hours of cold exposure (Dyson et al., 2016), amounts of citrate, malate and fumarate were determined to indicate whether analysed genotypes possess a similar and plausible range of organic acid concentrations (Figure SXII). While citrate amount fluctuated around the level of non-acclimated plants, fumarate and malate dynamics was affected by low temperature in all genotypes. Malate accumulated in all genotypes until Day 14 of cold acclimation, and most pronounced increase was observed in *f3h*, *bam3* and *pgm1*. In Col-0, the fumarate level under control conditions was higher than in the metabolic mutants, but its amount decreased significantly during cold acclimation. In *chs*, *f3h* and *bam3*, only slight dynamics of fumarate amount was observed during cold acclimation. Related to rates of net CO_2 assimilation, malate, fumarate and citrate

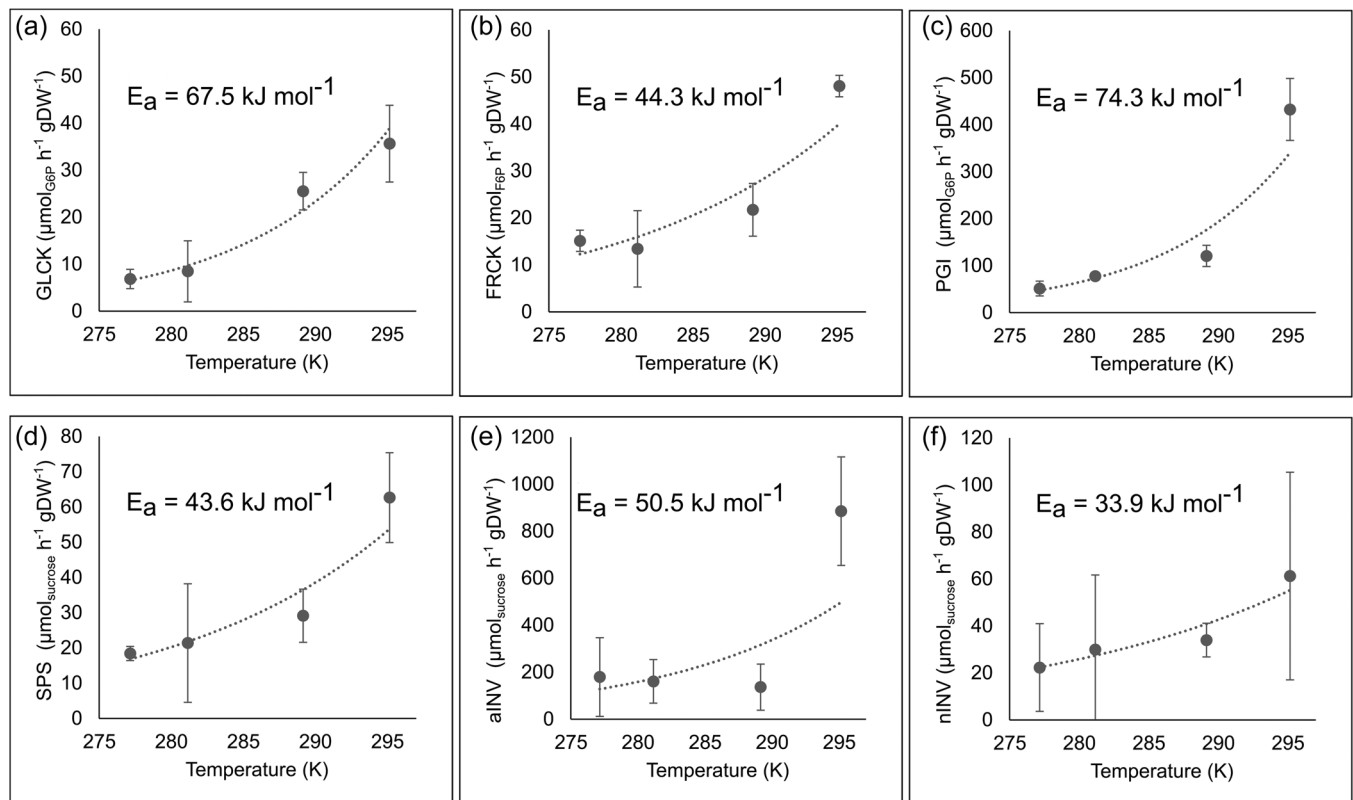


FIGURE 7 Temperature-dependency of maximum enzyme activities (v_{max}). (a) Glucokinase, GLCK; (b) fructokinase, FRCK; (c) phosphoglucoisomerase, PGI; (d) sucrose-phosphate synthase, SPS; (e) acidic invertase, aINV; (f) neutral invertase, nINV. Dashed line: exponential interpolation; vertical bars: standard deviation, $n \geq 3$; E_a : the activation energy. All measurements were performed with non-cold acclimated plants of Col-0.

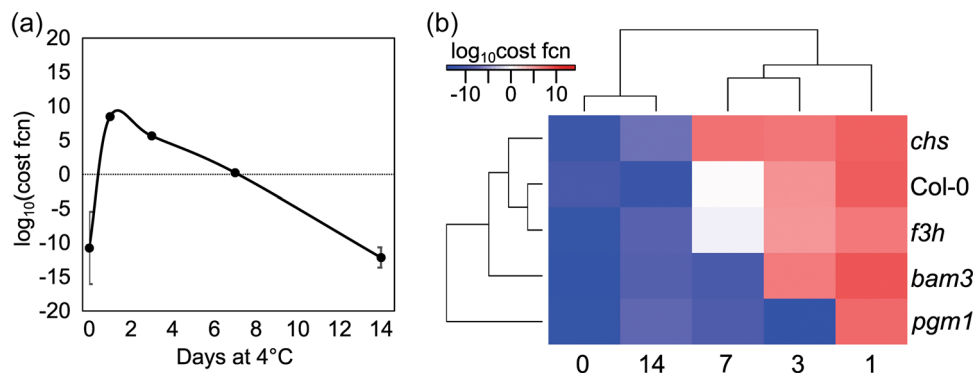


FIGURE 8 (a) Common logarithm of cost function (cost fcn) of an optimized kinetic model for Col-0 as a function of cold acclimation period. Shown are means \pm standard deviation ($n = 15$). (b) Hierarchical cluster analysis of mean cost functions (cost fcn) of optimized models (mean values of 15 global optimization runs). The \log_{10} values of cost functions are displayed in a heatmap and relationships between genotypes and days of acclimation are represented in a dendrogram based on Euclidean distances. [Color figure can be viewed at [wileyonlinelibrary.com](https://onlinelibrary.wiley.com/terms-and-conditions)]

accumulation was more pronounced in these three mutants than in Col-0 (Figure 9). In plants of starch deficient *pgm1* mutants, the fumarate amount increased twofold after 14 days of cold acclimation. In summary, cold-induced dynamics of quantified organic acid amount was found to be heterogeneous across all tested genotypes. The strongest increase of fumarate and malate amount between 0 and 14 days at 4°C was observed for starch deficient *pgm1* plants.

4 | DISCUSSION

Exposing plants of *Arabidopsis*, and many other species, to low, but nonfreezing temperature induces a multigenic process termed cold acclimation (Thomashow, 2010). Cold is perceived by sensing and signalling cascades which affect gene expression and metabolic regulation on various levels (Knight & Knight, 2012; Plieth et al., 1999;

Xin & Browse, 2000). Photosynthetic CO₂ uptake and metabolism of carbohydrates are directly affected by low temperature. As previously observed (Savitch et al., 2001), also in the present study cold exposure resulted in a decrease of F_v/F_m and net CO₂ assimilation rates while only minor differences were observed between analysed metabolic mutants (see Figures 2 and 3). This leads to the conclusion that, under conditions used in this study, neither starch deficiency in *pgm1* nor starch overaccumulation in *bam3* nor deficiency in anthocyanin accumulation (*chs*, *f3h*) have a significant impact on photosynthesis during cold acclimation. While for *pgm1* this is in line with previous findings (Sicher, 2011), such observation may only be valid under similar growth conditions with a low or mediate photosynthetic photon flux density (PPFD) of 100 $\mu\text{mol photons m}^{-2}\text{s}^{-1}$. Particularly, anthocyanins accumulate only in the cold if

(visible) light intensity or UVB radiation exceeds a certain threshold (Chalker-Scott, 1999). Carbon fixation within the CBBC results in sugar phosphates which are substrate for biosynthetic pathways of primary and secondary metabolism. While cold exposure typically induces both accumulation of carbohydrates and secondary metabolites (Doerfler et al., 2013), it remains unclear how carbon allocation into primary and secondary metabolism is regulated, and to which extend these two carbon flux branches depend on each other. Comparison of starch and anthocyanin amounts across all genotypes revealed a significant impact of both starch deficiency and overaccumulation on the capacity for anthocyanin accumulation, which was lower in both *pgm1* and *bam3* compared to Col-0 after 7 and 14 days of cold acclimation. In contrast, deficiencies in the anthocyanin pathway resulted in wild-type like starch amount (see Figure 4).

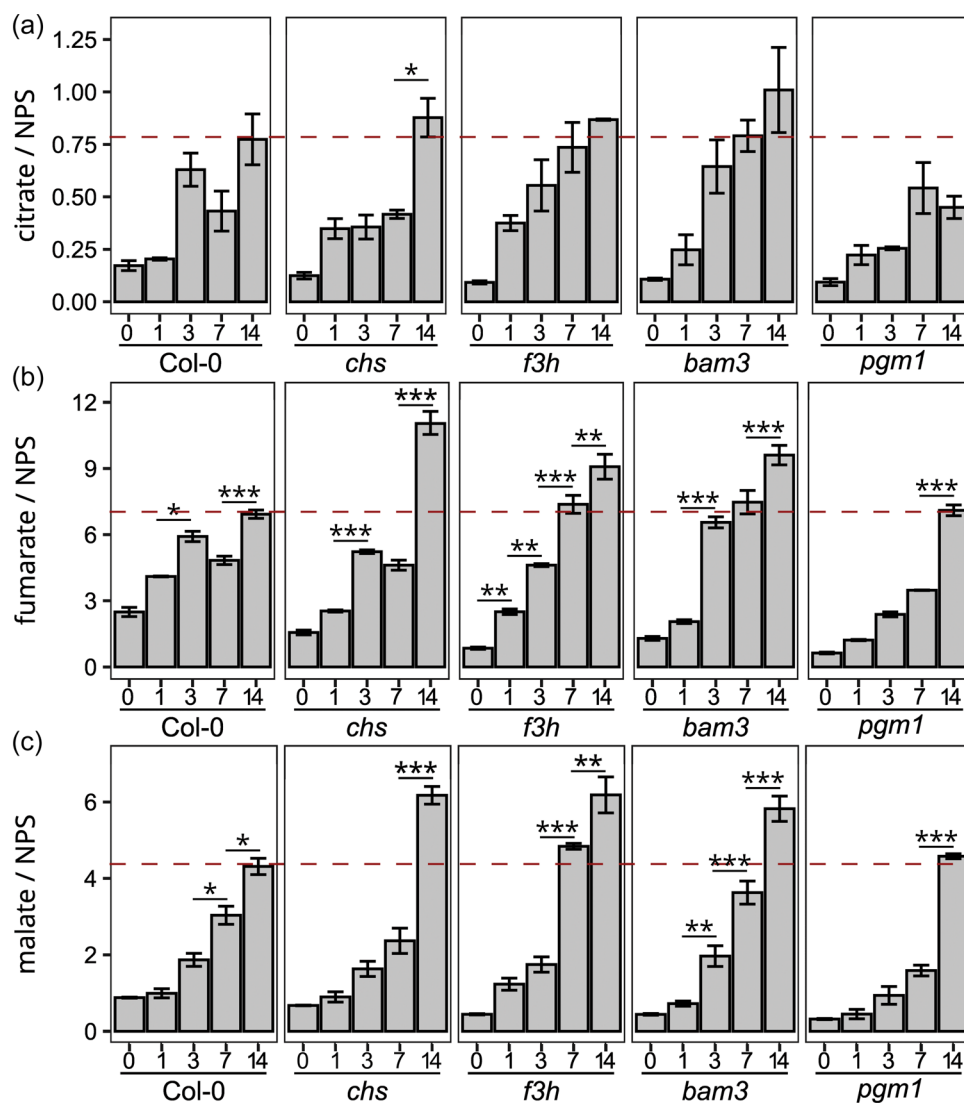


FIGURE 9 Quantitative ratio of organic acid amounts and net CO₂ uptake rates. (a) Ratio of citrate and NPS (in C₆/C₆ equivalents), (b) ratio of fumarate and NPS (in C₄/C₄ equivalents), (c) ratio of malate and NPS (in C₄/C₄ equivalents). NPS: net CO₂ assimilation. The red dashed line represents the mean maximum ratio in Col-0. Asterisks indicate significant difference between consecutive days within one genotype: *** $p < 0.001$; ** $p < 0.01$; * $p < 0.05$ (ANOVA with Tukey HSD, $n \geq 5$). More details about the ANOVA output are provided in Table SVIII. [Color figure can be viewed at wileyonlinelibrary.com]

Interestingly, amylase activity was significantly higher in *pgm1* than in Col-0 during the phase of strongest anthocyanin accumulation, that is, between 7 and 14 days (see Figure 6g). This might indicate that starch degradation represents a (metabolic) signal for induction of anthocyanin, or more general, flavonoid biosynthesis. While during the light phase, only a relatively small fraction of transitory leaf starch is degraded (Ishihara et al., 2022), this might be essential to maximise accumulation of flavonoids. Furthermore, it was interesting to observe that the complete flavonoid deficiency in *chs* was accompanied by increased mean growth rates which suggests impact of flavonoid accumulation on biomass accumulation in the cold. In addition, *chs* plants showed the most significant and strongest positive correlation of fresh and dry weight of plant shoot tissue. It remains speculation here but this observation might indicate (i) a role of flavonoids as osmolytes which affect tissue water content during cold acclimation, or (ii) modification of fluxes in metabolism redirecting carbon equivalents from flavonoid into cell wall biosynthesis. Furthermore, flavonoids have previously been suggested to play a central role for cold acclimation output, that is, freezing tolerance, in *A. thaliana* (Schulz et al., 2016). Consequently, reduced anthocyanin amounts of *bam3* and *pgm1* would be expected to result in reduced freezing tolerance. For *pgm1*, this has been shown before by electrolyte leakage assays, quantifying the LT50 of leaf tissue (Hoermiller et al., 2017). In *BMY8 (BAM3) RNAi lines*, freezing temperatures were found to affect F_v/F_m , that is, PSII integrity (Kaplan & Guy, 2005). In the present study, deficiency of flavonoids (in *chs*) was neither found to significantly affect F_v/F_m nor net CO₂ assimilation rates, which might be due to a relatively low/mild PPFD of 100 $\mu\text{mol photons m}^{-2}\text{s}^{-1}$, which only partially represents in situ conditions, for example, in the shade, of natural habitats (Callahan & Pigliucci, 2002; Nagler et al., 2018). Conclusively, the trade-off between stabilizing primary and energy metabolism and synthesising protective flavonoids in *Arabidopsis* needs to be studied under more challenging environments to quantify physiological effects of deficiencies in secondary metabolism and to validate the impact of starch degradation on flavonoid accumulation.

Amounts of starch and soluble carbohydrates are well known to (strongly) accumulate during cold acclimation despite a significant decrease of photosynthetic CO₂ uptake (Garcia-Molina et al., 2020; Guy et al., 2008; Hannah et al., 2006; Nägele et al., 2011; Nägele & Heyer, 2013; Savitch et al., 2001). This indicates a significant cold-induced reprogramming of plant metabolism to stabilize a new metabolic homeostasis and to prevent irreversible tissue damage (Kosová et al., 2011). Previous studies have shown that regulation of carbon allocation and flux partitioning between compartments, for example, chloroplasts and cytosol, plays a central role in cold acclimation because it enables compartment-specific accumulation of osmotically active and cryoprotective substances (Fürtauer et al., 2016; Hoermiller et al., 2017; Hoermiller et al., 2022; Lundmark et al., 2006). To reveal if and how deficiencies in starch and flavonoid metabolism may affect carbon partitioning during cold acclimation, substrate saturated enzyme activities, that is, v_{max} , of the central carbohydrate metabolism were quantified at different temperatures

ranging from ambient (22°C) to low (4°C) temperature. These experiments enabled a robust estimation of activation energy and kinetic modelling under a changing temperature regime (see Figure 7), except for acidic invertase where the Arrhenius assumption failed to predict experimental observations. This might indicate the necessity of purifying this invertase isoform to robustly estimate its kinetic under low temperature. Still, the estimated activation energy ($E_a = 50.5 \text{ kJ mol}^{-1}$) was similar to a commonly accepted range of many enzymes (40–50 kJ mol^{-1}), which still allowed for its application in kinetic models (Bisswanger, 2008). Kinetic simulations of a model comprising carbohydrate and anthocyanin metabolism failed in reproducing experimentally observed metabolite amounts during the initial cold acclimation phase between 1 and 3 days. In more detail, sucrose amount was significantly underestimated by model simulations, which was due to unbalanced sucrose biosynthesis and simulated export rates into other metabolic pathways. Introducing a second carbon efflux leaving the carbohydrate metabolism via the F6P pool could solve this problem across all time points and genotypes. Based on previous findings which showed SPS to catalyse a limiting metabolic step during cold acclimation (Nägele et al., 2012; Strand et al., 2003), simulation output suggested that SPS redirects carbon flux into other branches of primary metabolism, for example, glycolysis, tricarboxylic acid cycle, amino acid biosynthesis or respiration. The estimated carbon flux into the biosynthetic pathway of anthocyanins was of minor importance for solving this problem, which strengthens the hypothesis that flavonoid biosynthesis under growth conditions of the present study was not limited by carbon availability during cold acclimation. This estimation, however, is clearly based on the applied photometric approach for quantification of a C₁₅ backbone which might underestimate total C of anthocyanins (Saito et al., 2013), and also ignores diverse groups of flavonoids and secondary metabolites.

A plausible metabolic sink to solve the simulation and optimization problem was the pool of organic acids because its regulation has been described earlier to play an important role for cold acclimation (Dyson et al., 2016). Activity of the cytosolic fumarase enzyme FUM2 was found to be responsible for fumarate accumulation (Pracharoenwattana et al., 2010), and its deficiency prevents full acclimation of photosynthesis to low temperature (Dyson et al., 2016). Notably, FUM2 and SPS both are located within the cytosol, which might support the hypothesis that SPS limitation during cold acclimation enforces carbon partitioning in direction of fumarate biosynthesis without being accessible to the TCA cycle. As observed before (Hoermiller et al., 2017), fumarate amount was found to decrease during cold acclimation in Col-0. However, in relation to the total C assimilation flux quantified by NPS (see Figure 3), fumarate amount was increasing from a ratio of ~2.5 to ~7.5 (see Figure 9). The finding that these ratios reached highest values in *chs* (~11), *f3h* (~8.5) and *bam3* (~9) pointed to a role as alternative carbon sink during cold acclimation if capacities of starch and flavonoid accumulation were limited. Hence, while under ambient temperature (22°C) increased SPS activity in metabolic mutants could compensate for reduced carbon flux into starch and flavonoid pathways, cold-induced

de-regulation of starch and flavonoid metabolism may result in the need for additional alternative sinks, for example, organic acids. Finally, this finding suggests that carbon flux limitation by SPS induces a coordinate channelling during cold acclimation which supplies carbohydrates, organic acids and pathways of secondary metabolism in relation to carbon uptake rates for optimal energy supply under low temperature stress (Talts et al., 2004).

ACKNOWLEDGEMENTS

The authors thank the members of Plant Evolutionary Cell Biology at LMU Munich for many fruitful discussions. The authors thank AG Leister at LMU for support with spectrometer analysis. The authors also thank the Graduate School Life Science Munich (LSM) for support. This work was funded by Deutsche Forschungsgemeinschaft (DFG), grants TR175/C06 (to Andreas S. Richter) and TR175/D03 (to Thomas Nägele/Edda Klipp). Open Access funding enabled and organized by Projekt DEAL.

DATA AVAILABILITY STATEMENT

The data that support the findings of this study are available from the corresponding author upon reasonable request.

ORCID

Anastasia Kitashova  <https://orcid.org/0000-0002-4698-3255>

Andreas S. Richter  <https://orcid.org/0000-0002-2293-7297>

Edda Klipp  <https://orcid.org/0000-0002-0567-7075>

Thomas Nägele  <http://orcid.org/0000-0002-5896-238X>

REFERENCES

- Arrhenius, S. (1889) Über die Reaktionsgeschwindigkeit bei der Inversion von Rohrzucker durch Säuren. *Zeitschrift für physikalische Chemie*, 4, 226–248.
- Atanasov, V., Fürtauer, L. & Nägele, T. (2020) Indications for a central role of hexokinase activity in natural variation of heat acclimation in *Arabidopsis thaliana*. *Plants*, 9, 819.
- Austin, M.B. & Noel, J.P. (2003) The chalcone synthase superfamily of type III polyketide synthases. *Natural Product Reports*, 20, 79–110.
- Bisswanger, H. (2008) *Enzyme kinetics: principles and methods*. Weinheim: John Wiley & Sons.
- Callahan, H.S. & Pigliucci, M. (2002) Shade-induced plasticity and its ecological significance in wild populations of *Arabidopsis thaliana*. *Ecology*, 83, 1965–1980.
- Caretto, S., Linsalata, V., Colella, G., Mita, G. & Lattanzio, V. (2015) Carbon fluxes between primary metabolism and phenolic pathway in plant tissues under stress. *International Journal of Molecular Sciences*, 16, 26378–26394.
- Chalker-Scott, L. (1999) Environmental significance of anthocyanins in plant stress responses. *Photochemistry and Photobiology*, 70, 1–9.
- Cook, D., Fowler, S., Fiehn, O. & Thomashow, M.F. (2004) A prominent role for the CBF cold response pathway in configuring the low-temperature metabolome of *Arabidopsis*. *Proceedings of the National Academy of Sciences of the United States of America*, 101, 15243–15248.
- Doerfler, H., Lyon, D., Nägele, T., Sun, X., Fragner, L., Hadacek, F. et al. (2013) Granger causality in integrated GC-MS and LC-MS metabolomics data reveals the interface of primary and secondary metabolism. *Metabolomics*, 9, 564–574.
- Dyson, B.C., Miller, M.A.E., Feil, R., Rattray, N., Bowsher, C.G., Goodacre, R. et al. (2016) FUM2, a cytosolic fumarase, is essential for acclimation to low temperature in *Arabidopsis thaliana*. *Plant Physiology*, 172, 118–127.
- Falcone Ferreyra, M.L., Rius, S.P. & Casati, P. (2012) Flavonoids: biosynthesis, biological functions, and biotechnological applications. *Frontiers in Plant Science*, 3, 222.
- Ferreyra, M.L.F., Serra, P. & Casati, P. (2021) Recent advances on the roles of flavonoids as plant protective molecules after UV and high light exposure. *Physiologia Plantarum*, 173, 736–749.
- Fowler, S. & Thomashow, M.F. (2002) *Arabidopsis* transcriptome profiling indicates that multiple regulatory pathways are activated during cold acclimation in addition to the CBF cold response pathway. *The Plant Cell*, 14, 1675–1690.
- Fürtauer, L., Weckwerth, W. & Nägele, T. (2016) A benchtop fractionation procedure for subcellular analysis of the plant metabolome. *Frontiers in Plant Science*, 7, 1912.
- García-Molina, A., Kleine, T., Schneider, K., Mühlhaus, T., Lehmann, M. & Leister, D. (2020) Translational components contribute to acclimation responses to high light, heat, and cold in *Arabidopsis*. *iScience*, 23, 101331.
- Gibon, Y., Vigeolas, H., Tiessen, A., Geigenberger, P. & Stitt, M. (2002) Sensitive and high throughput metabolite assays for inorganic pyrophosphate, ADPGlc, nucleotide phosphates, and glycolytic intermediates based on a novel enzymic cycling system. *The Plant Journal*, 30, 221–235.
- Guy, C., Kaplan, F., Kopka, J., Selbig, J. & Hinch, D.K. (2008) Metabolomics of temperature stress. *Physiologia Plantarum*, 132, 220–235.
- Hannah, M.A., Heyer, A.G. & Hinch, D.K. (2005) A global survey of gene regulation during cold acclimation in *Arabidopsis thaliana*. *PLoS Genetics*, 1, e26.
- Hannah, M.A., Wiese, D., Freund, S., Fiehn, O., Heyer, A.G. & Hinch, D.K. (2006) Natural genetic variation of freezing tolerance in *Arabidopsis*. *Plant Physiology*, 142, 98–112.
- Havaux, M. & Kloppstech, K. (2001) The protective functions of carotenoid and flavonoid pigments against excess visible radiation at chilling temperature investigated in *Arabidopsis npq* and *tt* mutants. *Planta*, 213, 953–966.
- Hoermiller, I.L., Funck, D., Schönewolf, L., May, H. & Heyer, A.G. (2022) Cytosolic proline is required for basal freezing tolerance in *Arabidopsis*. *Plant, Cell & Environment*, 45, 147–155.
- Hoermiller, I.L., Naegel, T., Augustin, H., Stutz, S., Weckwerth, W. & Heyer, A.G. (2017) Subcellular reprogramming of metabolism during cold acclimation in *Arabidopsis thaliana*. *Plant, Cell & Environment*, 40, 602–610.
- Holaday, A.S., Martindale, W., Alred, R., Brooks, A.L. & Leegood, R.C. (1992) Changes in activities of enzymes of carbon metabolism in leaves during exposure of plants to low temperature. *Plant Physiology*, 98, 1105–1114.
- Huner, N.P.A., Öquist, G. & Sarhan, F. (1998) Energy balance and acclimation to light and cold. *Trends in Plant Science*, 3, 224–230.
- Ishihara, H., Alseekh, S., Feil, R., Perera, P., George, G.M., Niedźwiecki, P. et al. (2022) Rising rates of starch degradation during daytime and trehalose 6-phosphate optimize carbon availability. *Plant Physiology*, 189, 1976–2000.
- Kaplan, F. & Guy, C.L. (2004) β -Amylase induction and the protective role of maltose during temperature shock. *Plant Physiology*, 135, 1674–1684.
- Kaplan, F. & Guy, C.L. (2005) RNA interference of *Arabidopsis* beta-amylase8 prevents maltose accumulation upon cold shock and increases sensitivity of PSII photochemical efficiency to freezing stress. *The Plant Journal*, 44, 730–743.

- Kaplan, F., Kopka, J., Haskell, D.W., Zhao, W., Schiller, K.C., Gatzke, N. et al. (2004) Exploring the temperature-stress metabolome of *Arabidopsis*. *Plant Physiology*, 136, 4159–4168.
- Kitashova, A., Schneider, K., Fürtauer, L., Schröder, L., Scheibenbogen, T., Fürtauer, S. et al. (2021) Impaired chloroplast positioning affects photosynthetic capacity and regulation of the central carbohydrate metabolism during cold acclimation. *Photosynthesis Research*, 147, 49–60.
- Klotke, J., Kopka, J., Gatzke, N. & Heyer, A.G. (2004) Impact of soluble sugar concentrations on the acquisition of freezing tolerance in accessions of *Arabidopsis thaliana* with contrasting cold adaptation – evidence for a role of raffinose in cold acclimation. *Plant, Cell & Environment*, 27, 1395–1404.
- Knight, M.R. & Knight, H. (2012) Low-temperature perception leading to gene expression and cold tolerance in higher plants. *New Phytologist*, 195, 737–751.
- Korn, M., Peterek, S., Mock, H.-P., Heyer, A.G. & Hinch, D.K. (2008) Heterosis in the freezing tolerance, and sugar and flavonoid contents of crosses between *Arabidopsis thaliana* accessions of widely varying freezing tolerance. *Plant, Cell & Environment*, 31, 813–827.
- Kosová, K., Vítámvás, P., Prášil, I.T. & Renaut, J. (2011) Plant proteome changes under abiotic stress—contribution of proteomics studies to understanding plant stress response. *Journal of Proteomics*, 74, 1301–1322.
- Kötting, O., Pusch, K., Tiessen, A., Geigenberger, P., Steup, M. & Ritte, G. (2005) Identification of a novel enzyme required for starch metabolism in *Arabidopsis* leaves. The phosphoglucan, water dikinase. *Plant Physiology*, 137, 242–252.
- Leonardos, E.D., Savitch, L.V., Huner, N.P.A., Öquist, G., & Grodzinski, B. (2003) Daily photosynthetic and C-export patterns in winter wheat leaves during cold stress and acclimation. *Physiologia Plantarum*, 117(4), 521–531. <https://doi.org/10.1034/j.1399-3054.2003.00057.x>
- Lundmark, M., Cavaco, A.M., Trevanion, S. & Hurry, V. (2006) Carbon partitioning and export in transgenic *Arabidopsis thaliana* with altered capacity for sucrose synthesis grown at low temperature: a role for metabolite transporters. *Plant, Cell & Environment*, 29, 1703–1714.
- Monroe, J.D., Storm, A.R., Badley, E.M., Lehman, M.D., Platt, S.M., Saunders, L.K. et al. (2014) β -Amylase1 and β -amylase3 are plastidic starch hydrolases in *Arabidopsis* that seem to be adapted for different thermal, pH, and stress conditions. *Plant Physiology*, 166, 1748–1763.
- Nägele, T. & Heyer, A.G. (2013) Approximating subcellular organisation of carbohydrate metabolism during cold acclimation in different natural accessions of *Arabidopsis thaliana*. *New Phytologist*, 198, 777–787.
- Nägele, T., Kandel, B.A., Frana, S., Meißner, M. & Heyer, A.G. (2011) A systems biology approach for the analysis of carbohydrate dynamics during acclimation to low temperature in *Arabidopsis thaliana*. *FEBS Journal*, 278, 506–518.
- Nägele, T., Stutz, S., Hörmilller, I.I. & Heyer, A.G. (2012) Identification of a metabolic bottleneck for cold acclimation in *Arabidopsis thaliana*. *The Plant Journal*, 72, 102–114.
- Nagler, M., Nägele, T., Gilli, C., Fragner, L., Korte, A. & Platzer, A. et al. (2018) Eco-metabolomics and metabolic modeling: making the leap from model systems in the lab to native populations in the field. *Frontiers in Plant Science*, 9, 1556.
- Nagler, M., Nukarinen, E., Weckwerth, W. & Nägele, T. (2015) Integrative molecular profiling indicates a central role of transitory starch breakdown in establishing a stable C/N homeostasis during cold acclimation in two natural accessions of *Arabidopsis thaliana*. *BMC Plant Biology*, 15, 284.
- Niittylä, T., Messerli, G., Trevisan, M., Chen, J., Smith, A.M. & Zeeman, S.C. (2004) A previously unknown maltose transporter essential for starch degradation in leaves. *Science*, 303, 87–89.
- Oñate-Sánchez, L., & Vicente-Carbajosa, J. (2008). DNA-free RNA isolation protocols for *Arabidopsis thaliana*, including seeds and siliques. *BMC Research Notes*, 1(1), 93. <https://doi.org/10.1186/1756-0500-1-93>
- Owens, D.K., Crosby, K.C., Runac, J., Howard, B.A. & Winkel, B.S.J. (2008) Biochemical and genetic characterization of *Arabidopsis* flavanone 3 β -hydroxylase. *Plant Physiology and Biochemistry*, 46, 833–843.
- Plieth, C., Hansen, U.-P., Knight, H. & Knight, M.R. (1999) Temperature sensing by plants: the primary characteristics of signal perception and calcium response. *The Plant Journal*, 18, 491–497.
- Pracharoenwattana, I., Zhou, W., Keech, O., Francisco, P.B., Udomchalothorn, T., Tschoep, H. et al. (2010) *Arabidopsis* has a cytosolic fumarase required for the massive allocation of photosynthate into fumaric acid and for rapid plant growth on high nitrogen. *The Plant Journal*, 62, 785–795.
- Ristic, Z. & Ashworth, E.N. (1993) Changes in leaf ultrastructure and carbohydrates in *Arabidopsis thaliana* L. (Heyn) cv. Columbia during rapid cold acclimation. *Protoplasma*, 172, 111–123.
- Saito, K., Yonekura-Sakakibara, K., Nakabayashi, R., Higashi, Y., Yamazaki, M., Tohge, T. et al. (2013) The flavonoid biosynthetic pathway in *Arabidopsis*: structural and genetic diversity. *Plant Physiology and Biochemistry*, 72, 21–34.
- Savitch, L.V., Barker-Åstrom, J., Ivanov, A.G., Hurry, V., Öquist, G., Huner, N.P. et al. (2001) Cold acclimation of *Arabidopsis thaliana* results in incomplete recovery of photosynthetic capacity, associated with an increased reduction of the chloroplast stroma. *Planta*, 214, 295–303.
- Schulz, E., Tohge, T., Zuther, E., Fernie, A.R. & Hinch, D.K. (2015) Natural variation in flavonol and anthocyanin metabolism during cold acclimation in *Arabidopsis thaliana* accessions. *Plant, Cell & Environment*, 38, 1658–1672.
- Schulz, E., Tohge, T., Zuther, E., Fernie, A.R. & Hinch, D.K. (2016) Flavonoids are determinants of freezing tolerance and cold acclimation in *Arabidopsis thaliana*. *Scientific Reports*, 6, 34027.
- Seydel, C., Kitashova, A., Fürtauer, L. & Nägele, T. (2022) Temperature-induced dynamics of plant carbohydrate metabolism. *Physiologia Plantarum*, 174, e13602.
- Shi, M.-Z. & Xie, D.-Y. (2014) Biosynthesis and metabolic engineering of anthocyanins in *Arabidopsis thaliana*. *Recent Patents on Biotechnology*, 8, 47–60.
- Sicher, R. (2011) Carbon partitioning and the impact of starch deficiency on the initial response of *Arabidopsis* to chilling temperatures. *Plant Science*, 181, 167–176.
- Smith, A.M., Zeeman, S.C. & Smith, S.M. (2005) Starch degradation. *Annual Review of Plant Biology*, 56, 73–98.
- Stitt, M. & Hurry, V. (2002) A plant for all seasons: alterations in photosynthetic carbon metabolism during cold acclimation in *Arabidopsis*. *Current Opinion in Plant Biology*, 5, 199–206.
- Stitt, M. & Zeeman, S.C. (2012) Starch turnover: pathways, regulation and role in growth. *Current Opinion in Plant Biology*, 15, 282–292.
- Strand, Å., Foyer, C.H., Gustafsson, P., Gardeström, P. & Hurry, V. (2003) Altering flux through the sucrose biosynthesis pathway in transgenic *Arabidopsis thaliana* modifies photosynthetic acclimation at low temperatures and the development of freezing tolerance. *Plant, Cell & Environment*, 26, 523–535.
- Talts, P., Pärnik, T., Gardeström, P. & Keerberg, O. (2004) Respiratory acclimation in *Arabidopsis thaliana* leaves at low temperature. *Journal of Plant Physiology*, 161, 573–579.
- Thomashow, M.F. (2010) Molecular basis of plant cold acclimation: insights gained from studying the CBF cold response pathway. *Plant Physiology*, 154, 571–577.
- Vaz, A.I.F., & Vicente, L.N. (2007). A particle swarm pattern search method for bound constrained global optimization. *Journal of Global Optimization*, 39(2), 197–219. <https://doi.org/10.1007/s10898-007-9133-5>

- Weiszmann, J., Fürtauer, L., Weckwerth, W. & Nägele, T. (2018) Vacuolar sucrose cleavage prevents limitation of cytosolic carbohydrate metabolism and stabilizes photosynthesis under abiotic stress. *FEBS Journal*, 285, 4082–4098.
- Wiese, A., Gröner, F., Sonnewald, U., Deppner, H., Lerchl, J., Hebbeker, U. et al. (1999) Spinach hexokinase I is located in the outer envelope membrane of plastids. *FEBS Letters*, 461, 13–18.
- Winkel-Shirley, B. (2001) Flavonoid biosynthesis. A colorful model for genetics, biochemistry, cell biology, and biotechnology. *Plant Physiology*, 126, 485–493.
- Winkel-Shirley, B. (2002) Biosynthesis of flavonoids and effects of stress. *Current Opinion in Plant Biology*, 5, 218–223.
- Xin, Z. & Browse, J. (2000) Cold comfort farm: the acclimation of plants to freezing temperatures. *Plant, Cell & Environment*, 23, 893–902.
- Yano, R., Nakamura, M., Yoneyama, T. & Nishida, I. (2005) Starch-related α -glucan/water dikinase is involved in the cold-induced development of freezing tolerance in Arabidopsis. *Plant Physiology*, 138, 837–846.

- Yokoyama, R., de Oliveira, M.V.V., Kleven, B. & Maeda, H.A. (2021) The entry reaction of the plant shikimate pathway is subjected to highly complex metabolite-mediated regulation. *The Plant Cell*, 33, 671–696.

SUPPORTING INFORMATION

Additional supporting information can be found online in the Supporting Information section at the end of this article.

How to cite this article: Kitashova, A., Adler, S.O., Richter, A.S., Eberlein, S., Dziubek, D., Klipp, E., et al. (2023) Limitation of sucrose biosynthesis shapes carbon partitioning during plant cold acclimation. *Plant, Cell & Environment*, 46, 464–478. <https://doi.org/10.1111/pce.14483>